Facile synthesis of carbon nanotube/natural bentonite composites as a stable catalyst for styrene synthesis†

Ali Rinaldi,[ab] Jian Zhang,[a] Jan Mizera,[a] Frank Girgsdies,[a] Ning Wang,[c] Sharifah Bee Abd Hamid,[b] Robert Schlögl[a] and Dang Sheng Su*[a]

Received (in Cambridge, UK) 2nd September 2008, Accepted 20th October 2008
First published as an Advance Article on the web 11th November 2008
DOI: 10.1039/b815335c

Natural bentonite mineral, without any wet chemical treatment, was used directly to catalyze the growth of multi-wall CNTs and the produced CNTs/bentonite as an integrated composite stably catalyzed the oxidative dehydrogenation reaction over a long period of time; this concept provides a highly economical way for large-scale synthesis of nanocarbons and manufacture of styrene synthesis catalysts.

Supported iron is one of the most effective catalysts for the chemical vapor deposition (CVD) synthesis of carbon nanotubes.[1–4] Usually, Fe ions are artificially impregnated on supports and then activated by calcination–reduction treatments. The resulted iron nanoparticles are catalytically crucial to dissociate the hydrocarbon precursors and simultaneously serve as a structural template for the growth of tubular graphite.[5–9]

Bentonite, a cheap and abundant natural material, is a layered clay mineral in the aluminosilicate smectite family. In general, the most abundant elements in bentonite include O (28.6 wt%), Si (27.7 wt%), Fe (19.0 wt%), Al (9.6 wt%), Ca (6.8 wt%), Ti (3.3 wt%) and Mg (2.2 wt%) (Table S1, ESI†). The replacement of Al^{3+} by Mg^{2+} or Si^{4+} by Al^{3+} produces a negative charge, which would require a balance by the hydrated cations (Na^+ and/or Ca^{2+}). Water is thus able to enter into the interlayer to facilitate swelling and expanding the layers.[10] Its porosity can be further improved by exchanging with the polymeric metal or organo cations. The tunable surface and structural properties make ion-exchanged bentonite a good candidate as the catalyst support.[11] Application of clay minerals in CNTs synthesis has been reported,[12] but the catalyst preparation is still involved in depositing Fe ions onto the clay matrix. Actually, the Fe ions originally in the minerals can be directly used to catalyze the growth of nanocarbons.

Most recently, we have reported the successful application of the natural lava rock to catalyze the CNT synthesis.[13] Nanocarbons have also been found to efficiently catalyze the oxidative dehydrogenation (ODH) of ethylbenzene to produce styrene as a vital monomer in polymer industries.[14–17] In the present work, we show the superior performances of Fe-containing minerals in two important heterogeneous catalysis reactions: CNTs growth and ODH of ethylbenzene. The fabricated CNTs/bentonite composite displayed a high mechanical stability even after the ultrasonic treatment. As an ODH catalyst, it displayed a comparable activity to the commercial CNTs.

Commercial bentonite (Winston Company, Germany) was used as catalyst for CVD synthesis of CNTs without any treatment. 15 g of bentonite was placed in a rotating furnace (60 rpm) throughout the process. The temperature was raised to 700 °C at 10 °C min^{-1} in an He flow of 100 mL min^{-1}, and bentonite was reduced by 100 mL min^{-1} 75% H_2/He for 1 h. At the CVD process, a mixture of 60 mL min^{-1} C_2H_4 and 150 mL min^{-1} H_2 was introduced into the reactor for 1 h. Catalytic activity for ODH of ethylbenzene (EB) was evaluated at 400 °C under atmospheric pressure. 200 mg of sample was loaded in a fixed-bed quartz reactor and then the reactant (2.8% EB, O_2/EB = 2.5, He as balance) with a rate of 7.5 mL min^{-1} flowed the catalyst bed. Analysis of reactants and products was performed on a Varian CP-3800 gas chromatograph equipped with TCD and FID detectors. Commercial activated carbon (KD Tech, Malaysia) and multi-wall CNTs (Baytubes, Bayer MaterialScience AG, Germany) were also tested under same conditions. Chemical composition was analyzed by an X-ray fluorescence (XRF) spectrometer (Bruker AXS, S4 pioneer). X-Ray diffraction (XRD) spectra were obtained on a D8 ADVANCE diffractometer (Bruker AXS) using a secondary graphite monochromator (Cu-Kα_{1+2} radiation) and scintillation counter. BET surface area was measured by N_2 isotherm at 77 K (Quantachrome Instruments). The morphology of the sample was recorded with a Hitachi S4800 scanning electron microscope (SEM). Transmission electron microscopy (TEM) observations were carried out on a Philips CM200 LaB_6 and a CM200 FEG microscopes at 200 kV equipped STEM and EDAX detectors.

Distribution of each element in the fresh bentonite was analyzed by elemental mapping technique under the STEM mode. Fig. 1 showed a typical layered structure. The existence of Fe was clearly seen throughout of the sample. The XRF elemental analysis revealed that the bulk content of Fe is around 19 wt%. The existence of Ca and Na as the compensating ions was also identified.

Fig. 2 reports the powder XRD spectra of the fresh and reduced bentonites. For the fresh sample, two kinds of Fe-containing phases were observed, *i.e.* siderite [(Ca–Mg–Fe)CO_3] at $2\theta = 32.0°$ and armalcolite ($Fe_{0.5}Mg_{0.5}Ti_2O_5$) $2\theta = 25.5°$. After reduction, siderite almost disappeared with the presence of

[a] *Department of Inorganic Chemistry, Fritz Haber Institute of the Max Planck Society, Faradayweg 4-6, 14195 Berlin, Germany. E-mail: dangsheng@fhi-berlin.mpg.de; Fax: +49 30 8413 4401*
[b] *Combinatorial Technology & Catalysis Research Centre (COMBICAT), Block A, Level 3, Institute of Postgraduate Studies, University of Malaya, 50603, Kuala Lumpur*
[c] *Hongkong University of Science and Technology, Department of Physics, Clear Water Bay, Hongkong*
† Electronic supplementary information (ESI) available: XRF, BET, photograph, and TEM images. See DOI: 10.1039/b815335c

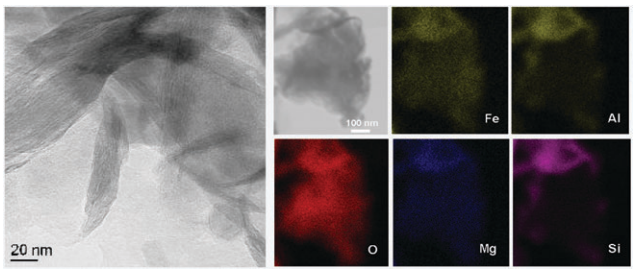

Fig. 1 TEM image (left, scale bar 20 nm) and elemental maps (right, scale bar 100 nm) of fresh bentonite.

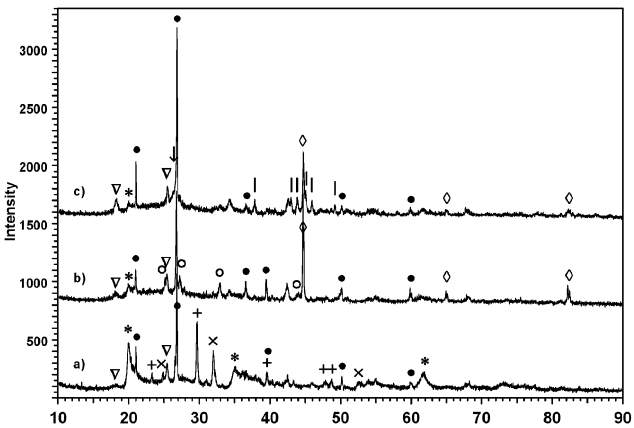

Fig. 2 XRD spectra of fresh bentonite (a), reduced-bentonite (b), and CNTs on bentonite (c) samples. (●) Low quartz SiO_2, (*) bentonite/smectite/montmorillonite, (▽) armalcolite $Fe_{0.5}Mg_{0.5}Ti_2O_5$, (+) magnesian calcite $(Ca,Mg)CO_3$, (×) (calcian/magnesian) siderite $(Fe,Ca,Mg)CO_3$, (○) vaterite μ-$CaCO_3$, (◇) metallic Fe, (|) Fe_3C, (↓) graphite.

metallic Fe at $2\theta = 44.7^\circ$. However, armalcolite is much less reducible and its intensity was retained even after CVD process, probably due to the low reducibility of the Fe–Ti spinel structure. Although it is difficult to fully rule out the role of armalcolite, we conclude that siderite is the major Fe source for CNTs growth. The intensity of peaks at $2\theta = 19.8^\circ$ and 35.3° decreased, revealing a partial collapse of the layered structure during the treatment.[18] After the CVD process, the Fe_3C phase appeared as metallic Fe vanished to a great extent, in accordance with the reports on the crucial role of Fe_3C for CNTs growth.[19]

A TEM image of the reduced bentonite sample is shown in Fig. 3(a), in which Fe nanoparticles were found in some typical areas. Stacking plate patterns revealed a partial destruction of the layered structure, resulting in a loss in porosity and thus a decrease of BET surface area from 88.7 to 10 $m^2\ g^{-1}$ (Table S2, ESI†). Fig. 3(b) and (c) show that the bentonite was covered by multi-wall CNTs after CVD process. Under the optimized conditions, the outer diameters of CNTs were between 5 and 40 nm (Fig. S1, ESI†). Such a wide range may be related with the chemical complexity of iron sources, *i.e.* siderite and armalcolite. As shown in the differential thermogravimetry (DTG) profile in the diluted O_2 flow (Fig. S1, ESI†), the composite is free of amorphous carbon peaking at the low-temperature zone and the combustion started at 420 °C, suggesting a high purity of CNTs in produced carbon with a yield of 28.7%. Fig. 3(d) gives the high-resolution image of the

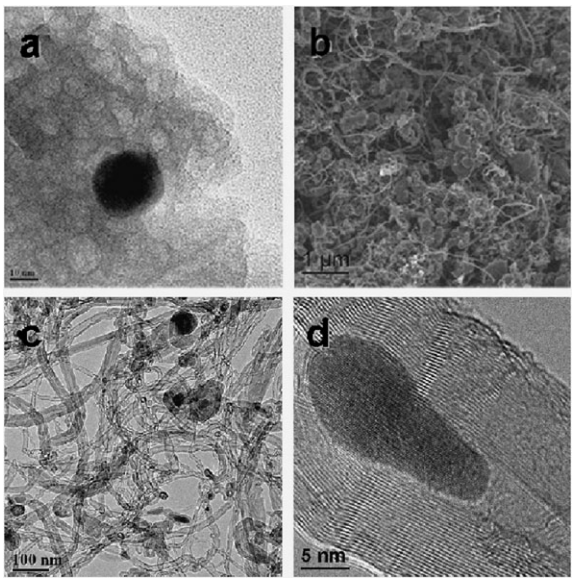

Fig. 3 SEM and TEM images of bentonite before and after CVD process: (a) reduced bentonite, scale bar 10 nm; (b) CNTs/bentonite composite, scale bar 1 μm; (c) produced CNTs, scale bar 100 nm; and, (d) CNTs-encapsulated Fe_3C nanoparticle, scale bar 5 nm.

encapsulated Fe_3C nanoparticle featuring a lattice distance of 0.21 nm. After the CVD process, the sample expanded to three times of its original volume (Fig. S2, ESI†). The obtained CNTs/bentonite composite possessed a surface area of 33.1 $m^2\ g^{-1}$, which is three times that of reduced bentonite. Growth of CNTs rebuilt the porosity to some extent, providing the possibility for its further application in catalysis.

The mechanical stability of the CNTs/bentonite composite was tested by the ultrasonic treatment. The sample was immersed into two types of solutions (*i.e.* water and hexane), and treated by the ultrasound for 2 h. As shown in Fig. 4(a), in water, the composite expanded to twice its original volume, leaving the liquid free of any visible suspended material. In hexane, the swelled composite almost filled the entire container, possibly due to the affinity of hexane to the hydrophobic surfaces of CNTs. The dispersed composite remained stable up to one week and the filtrate was free of observable particles. Nitrogen physisorption and SEM measurements did not show any observable change in either adsorption/desorption isotherms or overview morphologies (Fig 4(b)–(d)). A good mechanical stability of CNTs/bentonite composite is thus suggested.

We conducted the oxidative dehydrogenation of ethylbenzene on the as-synthesized CNTs/bentonite composite. One commercial CNTs and activated carbon were also tested for comparison. A carbon balance of 100 ± 3% was obtained in each test and the by-products were mainly CO_2 and CO due to the combustion. As shown in Fig. 5, the highest activity was observed on the activated carbon (AC) but gradually decreased along with the reaction. The weight gain of around 15 wt% on activated carbon indicated an irreversible coke formation over the whole period of reaction (see also the carbon balance in Fig. S3, ESI†). Obviously, it cannot meet the practical requirement on the long-time stability in chemical industries. Both CNTs/bentonite and commercial CNTs samples displayed an

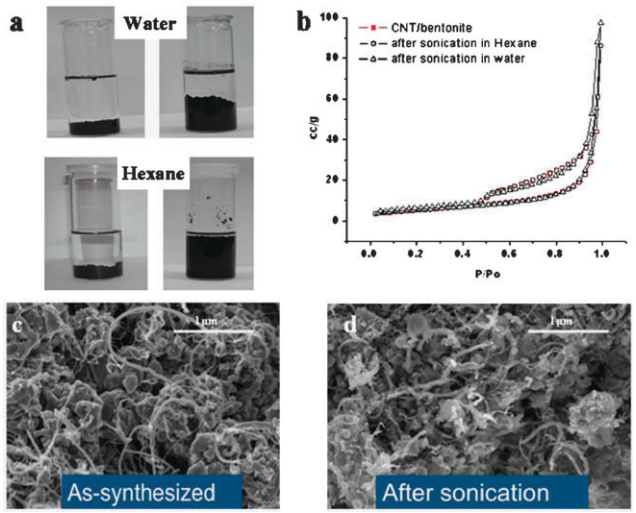

Fig. 4 Characterization of CNTs/bentonite composite. (a) Photographs of composites in water and hexane; (b) N_2 isotherms of samples before and after ultrasonic treatment for 2 h; and, (c–d) SEM images of samples before and after ultrasonic treatment in water, scale bar 1 μm.

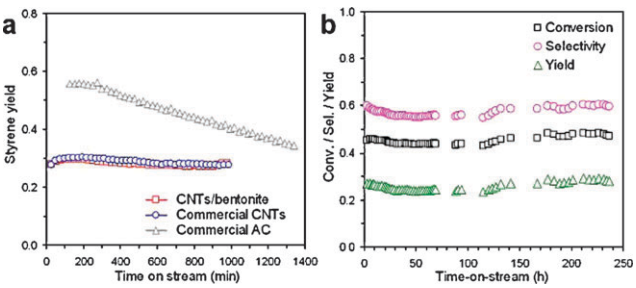

Fig. 5 Catalytic performance of CNTs/bentonite composition during ODH of ethylbenzene: (a) comparison with commercial CNTs and activated carbon (AC); and, (b) long-term stability. Reaction conditions: 0.2 g catalyst, 2.8% EB, O_2/EB = 2.5, 400 °C, 7.5 mL min^{-1}.

extremely stable performance, *i.e.* the yield to styrene remained at around 30%. An induction period can be found at the beginning, which might be due to O_2-assisted functionalization of the graphitic surface with oxygenated-surface groups as the active sites.[14,20] Especially for CNTs/bentonite, the ethylbenzene conversion, styrene selectivity and yield were almost unchanged during a reaction for 240 h. HRTEM images of the used sample shows that the Fe particles were well confined inside the graphitic shells (Fig. S4, ESI†) even after such a long period of time, evidencing the activity mainly originated from CNTs.

The styrene production rates based on the weight of catalyst were almost same for CNTs/bentonite and commercial CNTs samples, *i.e.* ~14.5 mmol/g_{cat}^{-1} h^{-1}. However, the measured bulk density of CNTs/bentonite (0.354 g cm^{-1}) was around two times of the commercial CNTs (0.175 g cm^{-1}) and thus the volumetric activities over CNTs/bentonite and commercial CNTs were 5.1 and 2.6 mmol cm^{-3} h^{-1}, respectively. It is known that the volume of an industrial reactor was usually strictly limited and the catalyst with a high bulk density would provide a high yield of the wanted products. From this viewpoint, CNTs/bentonite composite possessed a superior potential to the commercial CNTs. The economic properties of CNTs/bentonite also include the high utilization of carbon. After normalizing the styrene productivity to the content of carbon in the composite (*i.e.* 28.7%), we found that the activity was as high as 50.5 mmol/g_C^{-1} h^{-1}. Comparatively, the activity on the commercial CNTs was only 14.5 mmol/g_C^{-1} h^{-1}.

To conclude, we have shown the facile synthesis of CNTs composite and its application in catalysis. First, the cheap natural bentonite mineral can be directly used to catalyze the growth of CNTs, during which the naturally contained Fe serves as active phase and the layered oxides is the support. Second, the as-synthesized CNTs/bentonite composite efficiently catalyzed the ODH of ethylbenzene with a high volumetric productivity.

This work was financially supported by the EnerChem project of the Max Planck Society and CANAPE project of the 6th Framework Programme of European Commission. The authors thank Gisela Weinberg, Achim Klein and Wiebke Frandsen for technical works.

Notes and references

1 A. Fonseca, K. Hernadi, P. Piedirosso, J. F. Colomer, K. Mukhopadhyay, R. Doome, S. Lazarescu, L. P. Biro, P. H. Lambin, P. A. Thiry, D. Bernaets and J. P. Nagy, *Appl. Phys. A*, 1998, **67**, 11.
2 C. H. Laurent, A. Peigney and A. Rousset, *J. Mater. Chem.*, 1998, **8**, 1263.
3 K. Hernadi, A. Fonseca, J. B. Nagy, D. Bernaets, J. Riga and A. Lucas, *Synth. Met.*, 1996, **77**, 31.
4 K. Hernadi, A. Fonseca, J. B. Nagy, A. Siska and I. Kiricsi, *Appl. Catal. A*, 2000, **199**, 245.
5 A. C. Dupuis, *Prog. Mater. Sci.*, 2005, **50**, 929.
6 R. T. K. Baker, M. S. Kim, A. Chambers, C. Park and N. M. Rodriguez, in *Catalyst deactivation*, eds. C. H. Batholomew and G. A. Fuentes, Elsevier, Amsterdam, 1997, p. 99.
7 A. Gorbunov, O. Jost, W. Pompe and A. Graff, *Appl. Surf. Sci.*, 2002, **197**, 563.
8 H. Kim and W. Sigmund, *Carbon*, 2005, **43**, 1743.
9 A. R. Harutyunyan, T. Tokune, E. Mora, J.-W. Yoo and A. J. Epstein, *J. Appl. Phys.*, 2006, **100**, 44321.
10 S. Cheng, *Catal. Today*, 1999, **49**, 303.
11 Z. Ding, J. T. Kloprogge, R. L. Frost, G. Q. Lu and H. Y. Zhu, *J. Porous Mater.*, 2001, **8**, 273.
12 D. Gournis, M. A. Karakssides, T. Bakas, N. Boukos and D. Petridis, *Carbon*, 2002, **4**, 2641.
13 D. S. Su and X. Chen, *Angew. Chem., Int. Ed.*, 2007, **46**, 1823.
14 G. Mestl, N. I. Maksimova, N. Keller, V. V. Roddatis and R. Schlögl, *Angew. Chem., Int. Ed.*, 2001, **40**, 2066.
15 D. S. Su, N. I. Maksimova, N. Keller, G. Mesta, M. L. Ledoux and R. Schlögl, *Catal. Today*, 2005, **102–103**, 110.
16 J. J. Delgado, D. S. Su, G. Rebmann, N. Keller, A. Gajovic and R. Schlögl, *J. Catal.*, 2006, **244**, 126.
17 J. J. Delgado, R. Vieira, G. Rebmann, D. S. Su, N. Keller, M. L. Ledoux and R. Schlögl, *Carbon*, 2006, **44**, 799.
18 P. Cannizares, J. L. Valverde, M. R. Sun Kou and C. B. Molina, *Microporous Mesoporous Mater.*, 1999, **29**, 267.
19 A. Schaper, H. Hou, A. Greiner and F. Phillipp, *J. Catal.*, 2004, **222**, 250.
20 J. Zhang, D. S. Su, A. Zhang, D. Wang, R. Schlögl and C. Hérbert, *Angew. Chem., Int. Ed.*, 2007, **119**, 7460.

